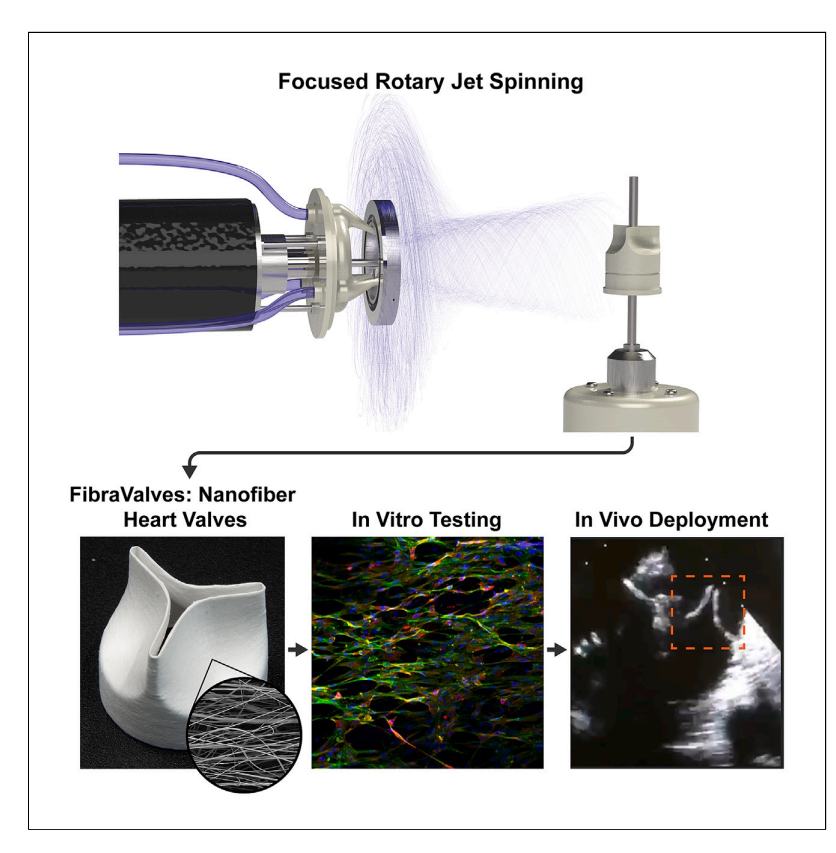
Matter



Article

On-demand heart valve manufacturing using focused rotary jet spinning



Many children suffer from heart valve diseases that necessitate valve replacement. Current heart valve replacement strategies do not grow alongside the patient and require repeat surgeries. Utilizing recent advances in fiber spinning, this work details FibraValves as a potential cardiac implant that will help patients regrow a native valve from their own cells. FibraValves were fabricated using focused rotary jet spinning and showed acute functionality in sheep, revealing the potential for clinical translation of this technology.

Sarah E. Motta, Michael M. Peters, Christophe O. Chantre, ..., Maximilian Y. Emmert, Simon P. Hoerstrup, Kevin Kit Parker

kkparker@g.harvard.edu

Highlights

Fabricated FibraValves that maintained unidirectional blood flow in vivo

Demonstrated focused rotary jet spinning as medical implant fabrication platform

Manufactured micro- and nanofiber scaffolds that mimic native valve mechanics

Spun fiber-based heart valve replacements in minutes



Motta et al., Matter 6, 1860–1879 June 7, 2023 © 2023 Elsevier Inc. https://doi.org/10.1016/j.matt.2023.05.025







Article

On-demand heart valve manufacturing using focused rotary jet spinning

Sarah E. Motta,^{1,2,3,8} Michael M. Peters,^{1,2,8} Christophe O. Chantre,^{1,2,8} Huibin Chang,^{1,2} Luca Cera,^{1,2} Qihan Liu,^{1,2} Elizabeth M. Cordoves,¹ Emanuela S. Fioretta,³ Polina Zaytseva,³ Nikola Cesarovic,^{4,5} Maximilian Y. Emmert,^{3,4,6,7} Simon P. Hoerstrup,^{2,3,6} and Kevin Kit Parker^{1,2,9,*}

SUMMARY

Pediatric heart valve disease affects children worldwide and necessitates valve replacements that remodel and grow with the patient. Current valve manufacturing technologies struggle to create valves that facilitate native tissue remodeling for permanent replacements. Here, we present focused rotary jet spinning (FRJS) for implantable medical devices, such as heart valves, to address this challenge. Combining RJS and a focused air stream, FRJS prints FibraValves, micro- and nanofibrous heart valves, in minutes. The micro- and nanoscale features provide structural cues to orient cells at the biotic-abiotic interface, while the centimeter-scale valve shape regulates cardiac flow. We built valves using poly(L-lactideco-E-caprolactone) fiber scaffolds, which supported rapid cellular infiltration and displayed native valve-like mechanical properties. Evaluating clinical translatability, we assessed acute performance in a large animal model using a transcatheter delivery approach. These tests indicate that FRJS is a viable method for manufacturing heart valves and future medical implants.

INTRODUCTION

Congenital and rheumatic heart disease are significant pediatric health issues, affecting roughly 12 million and 40 million children, respectively. ^{1–3} These patients often suffer from heart valve lesions and structural abnormalities, which necessitate cardiac interventions in the form of valve repair or replacement. ⁴ Heart valve replacements performed in children often require open heart surgeries and lifelong anticoagulation therapies. ^{5–7} Further, the pediatric valve recipients may outgrow the implant, thus requiring repeated interventions. ⁸

In efforts to provide a regenerative approach, tissue-engineered heart valves (TEHVs) have been suggested as a potential solution. ^{7,9–11} These valve replacements have shown initial promise, exhibiting remodeling capacities in acute and chronic large-animal models. ^{12–23} To promote tissue remodeling and self-repair, TEHV studies have primarily focused on fabricating scaffolds that mimic the extracellular matrix (ECM), a micro- and nanofibrous protein network that provides structure to tissues. The TEHV scaffolds allow the host's cells to infiltrate, proliferate, and remodel as heart valve tissue. ²⁴ Many traditional tissue engineering techniques utilize cell-based manufacturing to create ECM protein-based chemical cues that drive tissue remodeling *in situ*. ²⁵ Unfortunately, cell-based approaches, including cellularized and decellularized matrices, often take weeks to months to develop, making them costly and largely prohibitive. ²⁶

PROGRESS AND POTENTIAL

Children worldwide suffer from heart valve disease and often require open heart surgeries for valve replacements. Unfortunately, current heart valve replacements do not grow alongside the child, necessitating repeat high-risk surgeries throughout the pediatric patient's life. This work introduces FibraValves, heart valve replacements fabricated in minutes that comprise of fibers produced by focused rotary jet spinning. FibraValves are manufactured using biodegradable polymer fibers that allow for the patient's cells to attach and remodel the implanted scaffold, eventually building a native valve that can grow and live with the child throughout their life. These valves were tested in vitro and deployed in acute in vivo studies to evaluate their ability to maintain unidirectional blood flow in the heart. Together, these results suggest the potential translation of FibraValves as future cardiac implants, eliminating the need for repeated valve replacements in children.





Cell-free, synthetic in situ replacements require shorter fabrication times and have shown initial success maintaining valve function while allowing cellular infiltration and remodeling. 12,18,27-31 Synthetic heart valve scaffold manufacturing techniques include hydrogel molding, ³² 3D bioprinting, ³³ and fiber spinning. ³⁴ Hydrogel molding provides a customizable and reproducible method with facile manipulation of hydrogel material properties^{35,36}; unfortunately, molding-based processes do not recreate micro- and nanoscale size features characteristic of the ECM. Similarly, 3D printing approaches offer highly customizable and reproducible valve geometries^{33,37} but are unable to replicate the micro- and nanoscale features of valve scaffolds due to the trade-off between print resolution and production rate.³⁸ For fiber spinning techniques, electrospinning is commonly used to produce micro- and nanofiber sheets as ECM analogs. ^{27,30,39} Unfortunately, electrospinning is not able to recreate the 3D macroscale shape of the valve and requires post-processing to form the necessary leaflet geometries. Despite the distinguishing features of these fabrication methods, they do not achieve recapitulation of the valve ECM architectures in a cost- and time-efficient manner. Our group previously reported JetValves³¹ to address this issue; however, there were remaining improvements to be made in the manufacturing, fiber material, and valve geometrical design.

In this study, we sought to overcome these limitations by developing focused rotary jet spinning (FRJS)³⁸ for on-demand fabrication of customizable, native-like 3D heart valves. This system exploits centrifugal forces and focused air flow to engineer synthetic fibers and control their assembly via conformal deposition on a customizable valve collection mandrel. The rapid manufacturing capabilities of FRJS allow for the spinning of micro- and nanofibrous heart valve scaffolds (FibraValves) in less than 10 min, while the conformal collection supports the development of complex macroscale valve-shaped structures. We synthesized and tested a synthetic polymer, poly(L-lactide-co-&-caprolactone) (PLCL), in heart valve scaffolds, as it displayed native-like mechanical properties and allowed for increased cellular infiltration. Additionally, we investigated FibraValve performance in vitro, evaluating the valve's ability to regulate cardiac flow, and in vivo, assessing acute performance and functionality in a large-animal model using a transcatheter delivery approach. The use of the PLCL material, facilitating increased cellular infiltration, combined with the conformal deposition capabilities of FRJS enabled improved valve geometrical designs and performance compared with JetValves. These data suggest the effectiveness of FRJS as a manufacturing platform for on-demand production of medical implants.

RESULTS

Valve design strategy and manufacturing capabilities

Pulmonary valves are trileaflet valves characterized by a load-bearing micro- and nanofibrous collagen network with leaflet thicknesses of roughly 0.3–0.7 mm⁴⁰ (Figure 1A). Valvular function is maintained over millions of cycles due to the tissue's elastic properties and the leaflets' curved geometry, which combine to support physiological blood flow.^{40,41} We intended to design a pulmonary valve that was immediately functional after implantation and recapitulated key aspects of the native ECM to encourage cell infiltration. The design and production strategy included elastomeric polymer synthesis, mandrel printing, FibraValve spinning, and *in vitro* evaluation to ensure functionality prior to large-animal implantation (Figure 1B).

To fabricate micro- and nanofiber-based valve scaffolds, we utilized FRJS, ^{38,42} which allows for consistent, rapid, and reproducible production of polymeric fibers in the

¹Disease Biophysics Group, John A. Paulson School of Engineering and Applied Sciences, Harvard University, Boston, MA 02134, USA

²Wyss Institute for Biologically Inspired Engineering, Harvard University, Boston, MA 02115, USA

³Institute for Regenerative Medicine, University of Zurich, 8952 Schlieren, Switzerland

⁴Deutsches Herzzentrum der Charite (DHZC), Department of Cardiothoracic and Vascular Surgery, 13353 Berlin, Germany

⁵Department of Health Sciences and Technology, Swiss Federal Institute of Technology, 8092 Zurich, Switzerland

⁶Wyss Translational Center Zurich, University of Zurich and ETH Zurich, 8092 Zurich, Switzerland

⁷Charité Universitätsmedizin Berlin, 10117 Berlin, Germany

⁸These authors contributed equally

9I ead contac

*Correspondence: kkparker@g.harvard.edu https://doi.org/10.1016/j.matt.2023.05.025





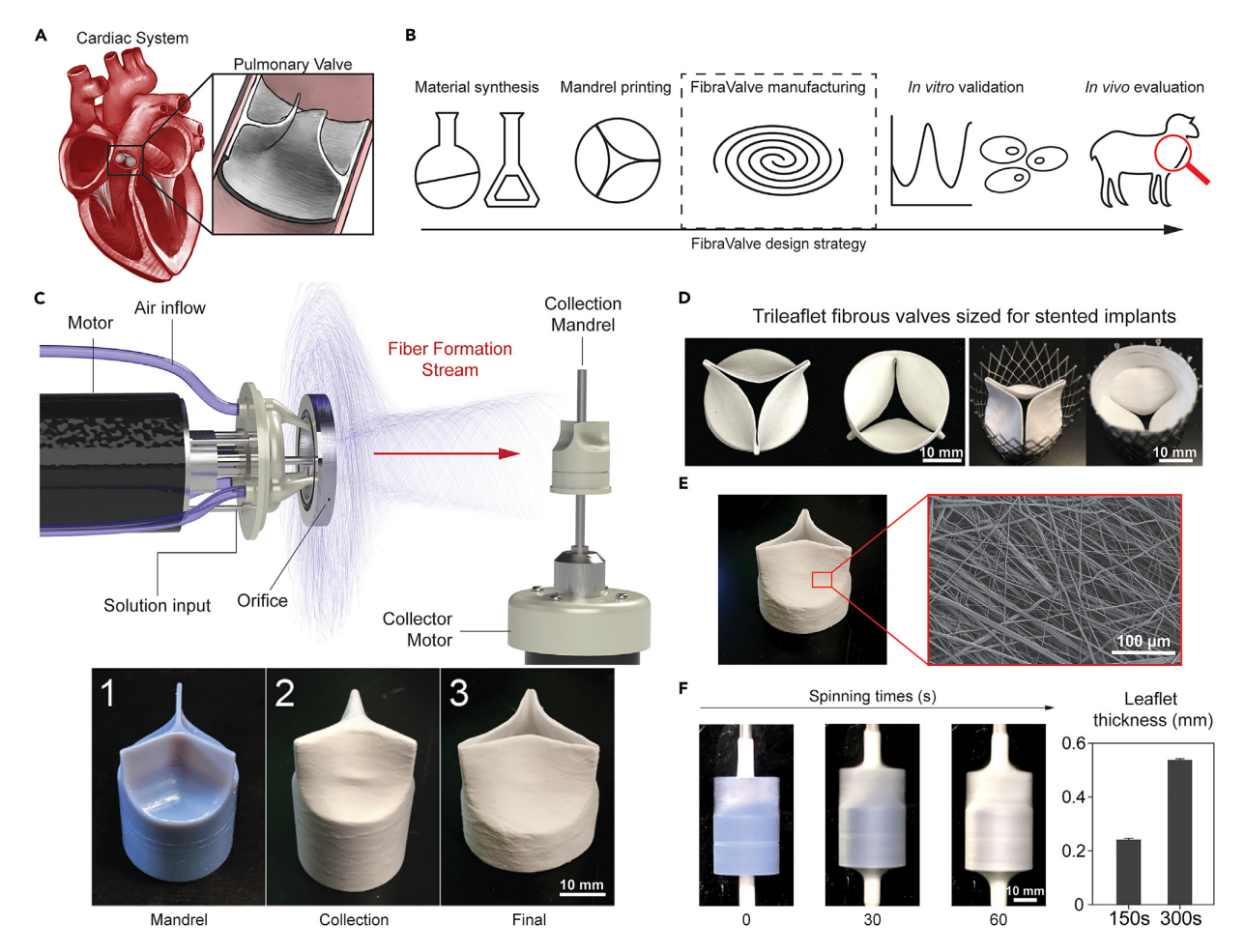


Figure 1. FibraValve design strategy and manufacturing capabilities

- (A) Heart valves, such as the pulmonary valve, regulate and control cardiac flow.
- (B) The design strategy to build a replacement valve shows an overview of the production and testing sequence that is often limited in the manufacturing portion.
- (C) The focused rotary jet spinning (FRJS) system allows for rapid polymer fiber deposition onto a collection mandrel via a focused air stream. The production process starts with an empty collection mandrel that is then coated with fibers before the valve is cut off and removed.
- (D) Designs are customizable and sized to be inserted into stents for implants.
- (E) The valves are fabricated from micro- and nanofibers that mimic the ECM.
- (F) Manufacturing times for valves on the FRJS system are on the scale of minutes. Thickness measurements were taken on the leaflet portion of the valve after spinning fibers for the indicated amount of time (n = 3 valves). Error bars represent standard error of the mean.

form of 3D valvular scaffolds (Figures 1C and S1). For FRJS, similar to previous RJS-based platforms, $^{43-45}$ centrifugal forces generate micro- and nanoscale fibers from a synthetic polymer solution. The FRJS consists of a high-speed rotating reservoir that extrudes polymer jets through orifices (diameter = 400 μm) on its side wall. Radial centrifugal forces expel the polymer solution through the orifices and into elongated jets. 45,46 The polymer jets extend into thin liquid streams where there is concurrent polymer chain entanglement and solvent evaporation, in turn forming continuous fibers. 47 During fiber formation, the polymer solution's viscosity resists potential beading caused by surface tension of the solvent. 48 To improve collection efficiency, the FRJS system employs a focused air jet positioned behind the rotating reservoir to direct the fibers into a focused stream onto the valve-shaped collection mandrel.



The valve scaffolds are then embossed (while still on the collection mandrel) to create deeper curvature in the leaflets (Figure S2D). This FibraValve manufacturing process allows for minimal manufacturing steps: (1) mandrel design, (2) fiber scaffold collection, (3) leaflet embossing, and (4) trimming and suturing into a final shape (Figures 1C and S2).

Leveraging this manufacturing capability, fibrous pulmonary valve scaffolds can be produced (Figure 1). The seamless collection method allows for the creation of entire valve geometries without reliance on post-processing of flat fiber sheets, which is necessary for other fabrication techniques. 12,13,16 Processing of these flat sheets includes physical modifications (such as bending, folding, and suturing) that may potentiate discontinuities, inconsistencies in properties such as leaflet shape, and delamination in the prosthesis. Scanning electron micrographs revealed the overall circumferential alignment of the fibers, induced by rotating the collection mandrel (Figure S3). This anisotropic organization mimics the directionality of the loadbearing circumferential collagen network found in the fibrosa layer of the native valve leaflet. 31,40 The Fibra Valve's circumferential alignment is lower than the anisotropy of the native fibrosa layer. However, the crosshatch fiber assembly ensures biaxial loading capabilities that, in the native valve leaflet, are provided by the ventricularis layer, composed mostly of radially aligned elastin fibers. 49 After spinning and suturing into a nitinol stent, the valves showed a homogeneous surface without delaminating fibers (Figure 1D). The fiber production capabilities of FRJS enabled the spinning of valves with 0.5 mm wall thickness (total valve weight: ~1 g) in less than 10 min (Figure 1F; Video S1). FibraValves were fabricated with production rates up to 0.2 g/min, orders of magnitude faster than electrospinning systems (between 0.000167 and 0.0167 g/min)⁵⁰ typically used for fiber-based tissue engineered scaffold development, including heart valves²⁷ and blood vessels.⁵¹ The FRJS system offers two important capabilities: control over multiscale resolutions, from micro- and nanofiber spinning to complex scaffold geometries on the centimeter scale, and a high fiber production rate, enabling rapid manufacturing.

Scaffold design, characterization, and in vitro testing

An *in situ* regenerative heart valve scaffold should present soft and elastic properties to support the mechanical stimuli experienced by the valve, including tensile strains of 9%–25% and tensile stresses of 21–80 kPa (stress values calculated for the pulmonary valve; Equation S1). ^{41,52,53} The scaffolds should also maintain a porous structure that permits rapid cellular infiltration and tissue remodeling. Purely synthetic scaffolds, including supramolecular approaches, have been investigated in long-term (up to 2 years) *in vivo* studies with different designs and showed mixed results. ^{27,54} Evidence of calcium deposits and leaflet shortening suggest that these synthetic approaches suffer from excessive inflammatory responses at the biotic-abiotic interface and biodegradation timescales that are mismatched to the tissue remodeling and regeneration. ⁵⁵

Among these synthetic polymer-based approaches, polycaprolactone (PCL) is a common biodegradable material used in heart valve tissue engineering. ^{56,57} Here, PCL was used in combination with polylactic acid (PLA) to synthesize a PLA:PCL multiblock copolymer termed PLCL, an elastomeric polyester for FibraValves. Previous studies indicated that PLCL formulations exhibited timely biodegradation, approximately 6 months in rats, and functional tissue remodeling. ⁵¹ A 4,000:2,000 molecular weight ratio of PLA:PCL was selected as it consistently formed fibers in the FRJS that displayed the desired elastic properties (Figures 2 and S4). The PLA





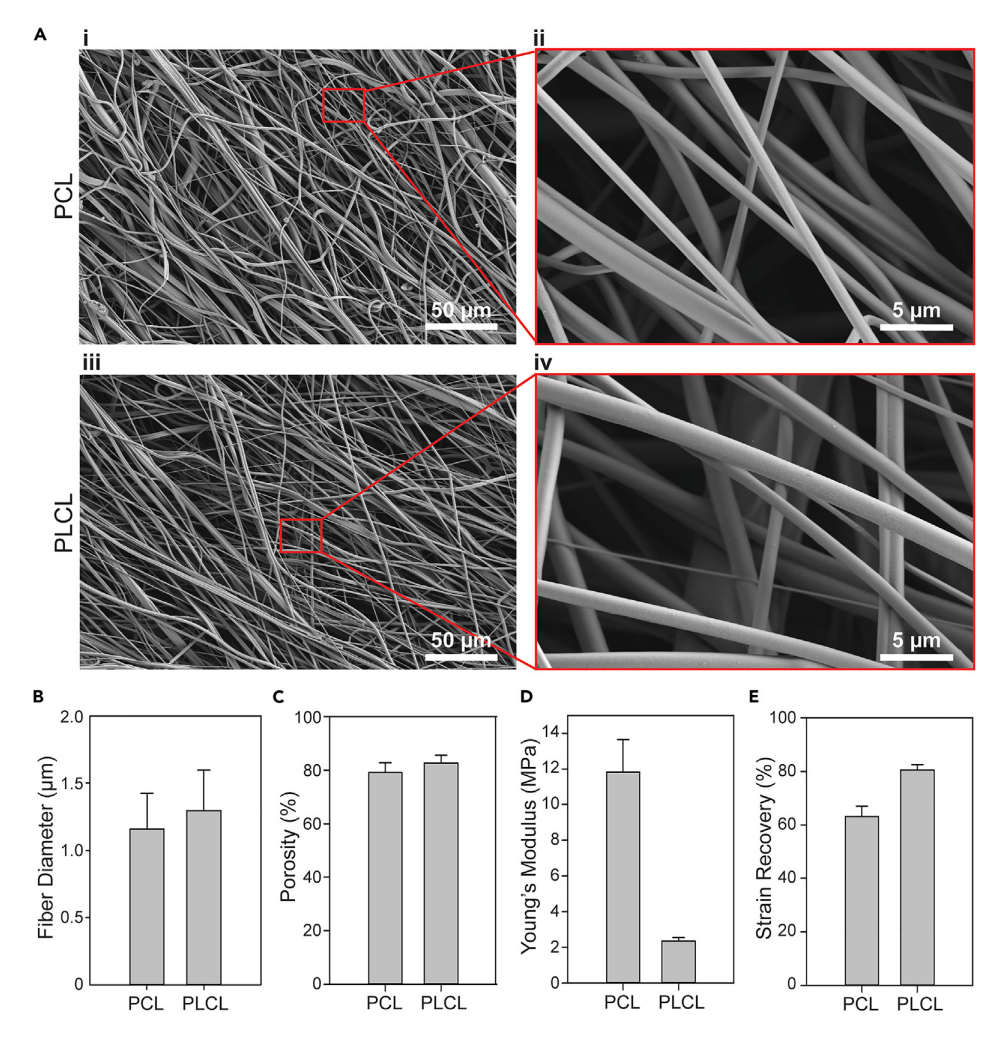


Figure 2. Elastomer fiber scaffolds design and mechanical and structural characterization
(Ai–Aiv) PCL (Ai and Aii) and PLCL (Aiii and Aiv) fiber scaffolds displayed similar fiber morphology as seen in the SEM images.

(B and C) Both PCL and PLCL scaffolds had similar fiber diameters that spanned the nano-micrometer size range (n = 3 scaffolds with 50 fibers per scaffold) as well as high scaffold porosity (n = 7 scaffolds).

(D and E) The scaffolds differed as the softer PLCL showed lower Young's modulus but higher strain recovery than the PCL fibers (n = 10 scaffolds). All error bars represent standard error of the mean.

(hard block) and PCL (soft block) combination with equal molecular weights has been shown to display high elasticity and moderate degradation rates. ⁵⁸

For all proceeding tests, PCL fiber scaffolds were used as a control. Throughout scaffold production, the PLCL copolymer was spun with average fiber sizes of $\sim\!1.3~\mu m$ with fiber diameters ranging from 500 nm to 5 μm (Figures 2A and 2B). These PLCL fibers assembled into scaffolds with porosities measuring above 80% (Figure 2C), similar to the PCL scaffold controls. Fibrous scaffolds fabricated with PLCL showed a Young's modulus of $\sim\!2.5$ MPa and a high strain recovery of $\sim\!80\%$, making them softer than PCL scaffolds ($\sim\!12$ MPa modulus) and $\sim\!20\%$ more efficient in strain recovery (Figures 2D, 2E, and S5). The PLCL scaffolds are in the range of native valves (1–12 MPa)⁵³ but are softer than previously reported polymer-based TEHVs ($\sim\!11$ MPa). Compared with PCL scaffolds, the PLCL fiber scaffolds demonstrated



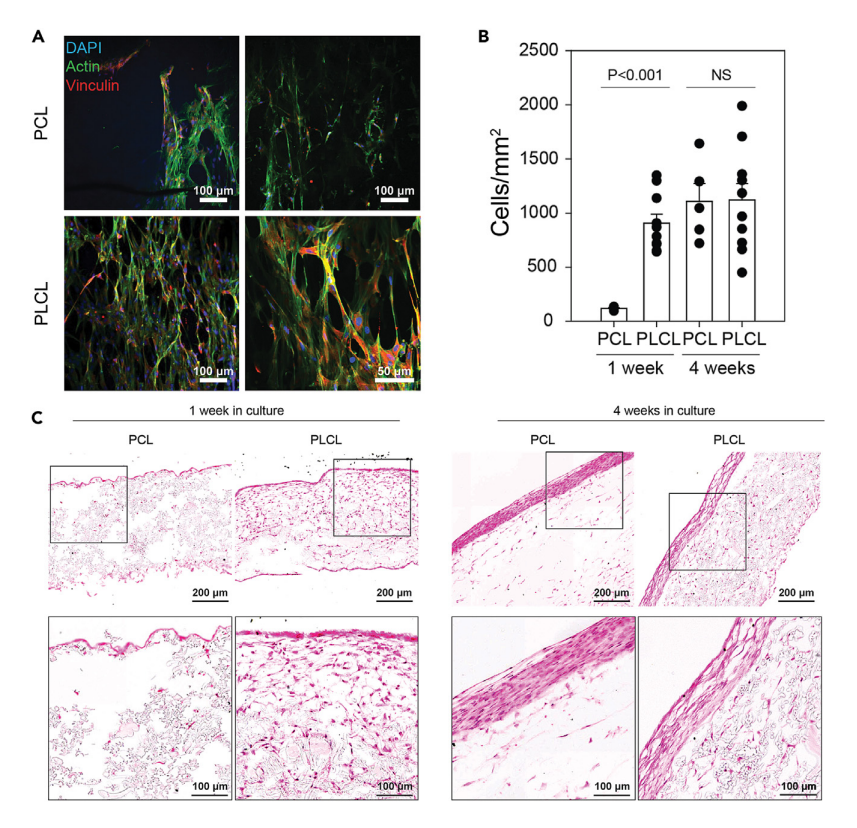


Figure 3. Scaffolds in vitro testing reveal rapid cellular adhesion and infiltration

- (A) Representative immunofluorescent images, stained for DAPI, actin, and vinculin, reveal an improved adhesion of VICs on PLCL fibers, with stronger presence of focal adhesions (vinculin stain). Images were taken after 2 days *in vitro*.
- (B) Quantification of cells per area in the scaffolds shows a significant difference between the PCL and the PLCL scaffolds at 1 week. At 4 weeks, infiltration is equivalent (n=5 scaffolds for the PCL and n=10 scaffolds for the PLCL; error represents standard error of the mean).
- (C) Representative H&E histology sections of VICs cultured on fiber scaffolds for 1 and 4 weeks. PLCL scaffolds at 1 week show full-thickness infiltration of VICs and limited infiltration in PCL scaffolds. At 4 weeks, both scaffolds show similar infiltration and formation of neotissue on the surface.

softer and more elastic mechanical properties while maintaining equivalent porosity (Videos S2 and S3).

These PLCL scaffolds were designed to mimic the structural and mechanical properties of native valve ECM to withstand the hemodynamic pressures of the heart. Additionally, the scaffold material can influence cellular behavior and remodeling. Therefore, cellular adherence and morphology on the different scaffold types was evaluated shortly after seeding (48 h), and cellular infiltration into the scaffolds was quantified at 1 and 4 week time points post-seeding. Cell-based *in vitro* studies utilized valvular interstitial cells (VICs) isolated from sheep heart valves. To assess VIC adhesion and morphology, cells were seeded onto large PCL and PLCL fiber strips (5 \times 20 \times 0.5 mm) and cultured for 2 days before they were stained and imaged for vinculin and F-actin (Figure 3A). Images revealed large areas of cellular confluence for both conditions, with more homogeneous coverage and elongated cell morphologies for the PLCL scaffolds.





Next, VIC infiltration into the different scaffolds was evaluated after 1 and 4 weeks of culture to provide more information on the cell-scaffold interface. Histological sections (cut orthogonal to fiber direction) stained with hematoxylin and eosin (H&E) were used for this evaluation. After 1 week of culture, a significantly higher number of cells was observed inside the PLCL scaffolds compared with the PCL scaffolds (Figure 3B). This increase in cell number was also characterized by a more homogeneous distribution evident in the H&E images (Figure 3C). After 4 weeks, both PCL and PLCL scaffolds showed similar levels in terms of total cell population (Figure 3B). However, the PLCL scaffolds showed a more homogeneous distribution of VICs throughout the scaffold thickness, whereas the PCL scaffolds displayed a dense formation of cells on the scaffold surface (Figure 3C). Mechanical testing of scaffolds cultured for 4 weeks revealed slightly softer mechanical properties and similar elastic properties to as-spun scaffolds (Figure S6). Altogether, these data revealed high *in vitro* cell adhesion and proliferation for the PLCL scaffolds and their potential ability to sustain rapid endogenous cell infiltration.

FibraValve geometry design and functional testing

Recent studies investigating the function and regenerative capacity of tissue-engineered valve scaffolds in long-term studies (up to 12 months) revealed the importance of appropriately designing the valve geometry. ^{22,27,60,61} Dimensions including leaflet curvature, leaflet length, and leaflet height (Figures 4Ai and 4Aii) are crucial and contribute to the formation of the coaptation area, the region where the inner (ventricle-facing) surface of the leaflets join while the valve is closed (Figure 4Aiii). These aspects are critical in supporting valvular function and physiological hemodynamics. ²² In some implantations, failure to achieve an effective combination of these valve geometries, regardless of fabrication method, may potentiate pathological remodeling, including leaflet retraction and valvular incompetence. ^{16,17,19,22,61} Based on these insights, we reasoned that FRJS's rapid manufacturing and design iteration capabilities could be leveraged to screen multiple valve scaffold geometries and subject them to physiological pulmonary pressures using an *in vitro* valve tester (pulse duplicator system), prior to costly *in vivo* studies

Previously, we reported synthetic fiber-based biomimetic semilunar heart valves that lacked a sufficient coaptation area (0 mm coaptation height at the center; Figure S7). The lack of coaptation in the valve shape led to moderate/high regurgitation *in vitro* (greater than 30%) and minor regurgitation *in vivo* (acute study in sheep). Here, we sought to design FibraValves with different leaflet geometries and sizes to vary the valves' coaptation areas. We developed four FibraValve designs: short (S), medium (M), long (L), and extra-long (XL) with different leaflet lengths (LLs), heights (Hs), and curvatures (Rs) (Figures 4A and 4B). The M, L, and XL designs exhibited increasing leaflet sizes and coaptation areas, while the S design was based on the previously published valve, which showed a lack of coaptation area. In the sufficiency of the sufficiency of

The M, L, and XL designs displayed coaptation areas, as adjacent leaflets touched while at rest (Figure 4B). Despite the increased coaptation area when compared with the S design, the FibraValve M exhibited a small opening in the center, whereas the L and XL designs had coaptation across the full LL (Figure 4B). When subjected to pulmonary pressures inside the pulse duplicator system, the elastic nature of the of the PLCL valves allowed for leaflet bending in the M design that created coaptation across the full LL, whereas the S design still possesses the central gap (Figure 4B; Videos S4, and S5). With the coaptation across the full LL, the FibraValve M showed

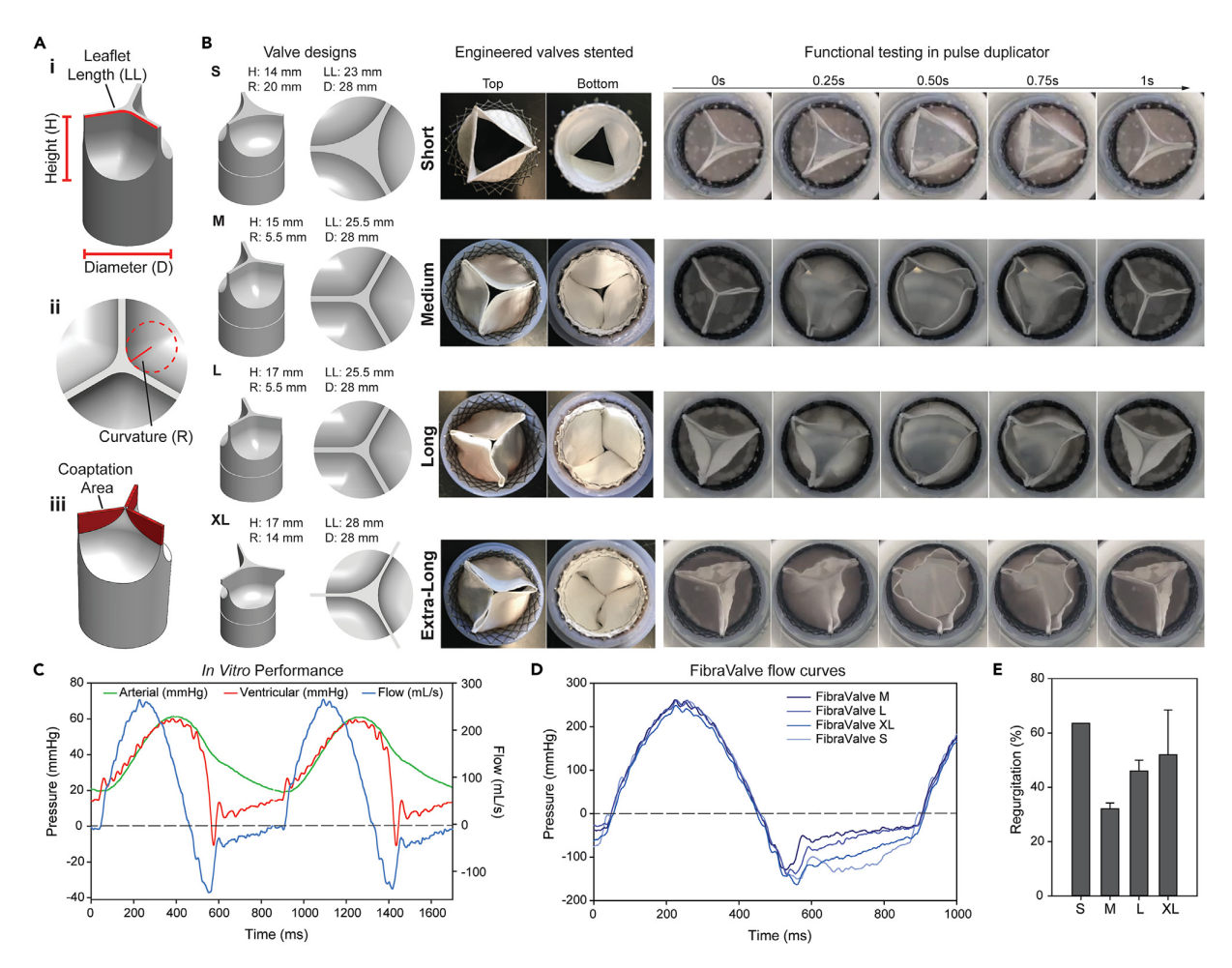


Figure 4. FibraValve design and functional testing reveal optimal design geometry

(Ai–Aiii) FibraValve molds were fabricated with varied parameters in the (Ai) height (H), leaflet length (LL), diameter (D), and (Aii) radius of curvature (R). (Aiii) These parameters combine to form different coaptation areas, the portion where the inner side of the leaflets contact each other.

(B) The valve mold was 3D printed with the indicated dimensions in preparation for fiber spinning. The valves were sized to fit inside a stent and recreate the physiological tri-leaflet shape. Valves were subjected to *in vitro* functional testing in a pulse duplicator, which recreates cardiac pressures and flows. Imaging throughout the systolic and diastolic phases shows typical leaflet movement throughout the cardiac cycle.

(C) Arterial and ventricular pressures as well as fluidic flows were recorded and are shown for the M valve design.

(D and E) For each valve design, (D) flow curves were recorded and (E) used to calculate the regurgitation levels for each FibraValve shape (n = 7 for M and n = 2 for all other conditions; error represents standard error of the mean).

30% regurgitation (Figures 4C–4E). Although 30% is considered moderate, a large fraction of this regurgitation was caused by water (low viscosity compared with blood) perfusing through the porous scaffold. When FibraValve M was spun using a blend of polymer and gelatin (85:15 ratio) to reduce permeability, regurgitation decreased to \sim 16% (Figure S8). By further increasing the gelatin fraction to 60:40, regurgitation continued decreasing to \sim 13% (Figure S8). These results suggest that the increased coaptation area of the M design compared with the S design led to lower regurgitation levels.

To mitigate valve leaflet shortening observed in long-term studies,^{22,27,54} the FibraValves L and XL were designed with longer and wider leaflets. However, the larger leaflets collapsed, with the leaflets folding back onto themselves. This





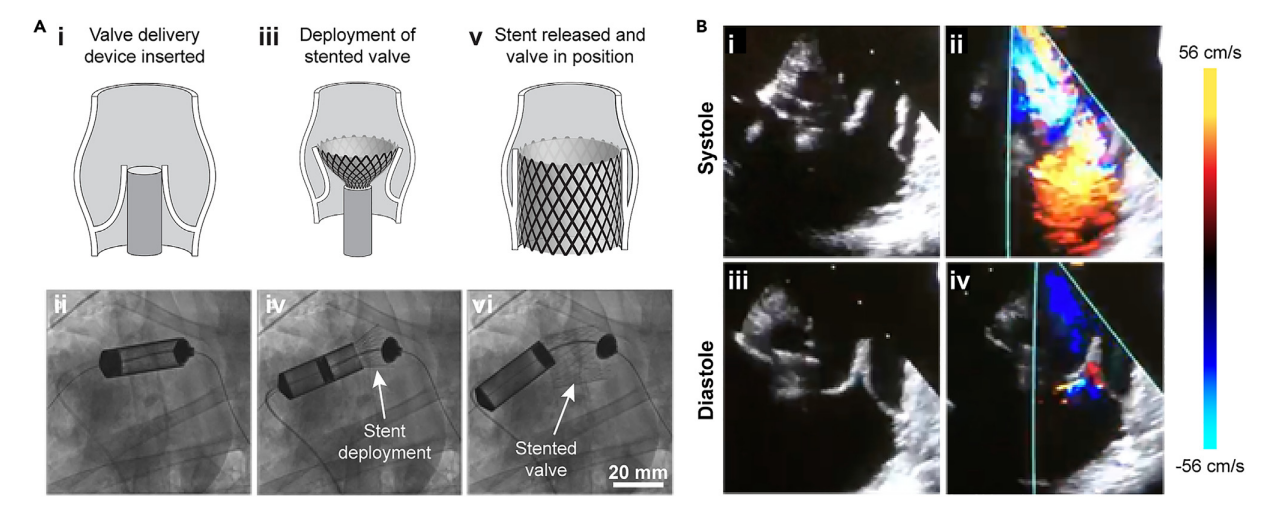


Figure 5. Transapical delivery of a FibraValve into pulmonary position under fluoroscopy guidance and echocardiographic evaluation
(Ai and Aii) Upon imaging the native pulmonary root, the FibraValve delivery system was inserted and aligned to the implantation site.
(Aiii and Aiv) When in the desired position, the stent is deployed, expanding to allow for valve placement and operation.
(Av–Avi) Eventually, the stent is fully deployed, holding the replacement valve in place via radial forces pressing the native valve leaflets against the root wall.

(Bi–Biv) Echocardiographic assessment of valve functionality in vivo showing correct leaflet motion and performance during systole (Bi and Bii) and diastole (Biii and Biv).

abnormal leaflet movement led to higher regurgitation, \sim 45% for the L design and \sim 50% for the FibraValve XL (Figures 4B, 4D, and 4E; Videos S6 and S7). While the L and XL designs were closer in dimension to native valve leaflets, ⁴⁰ their *in vitro* regurgitation levels were higher than the M design. The L and XL designs were therefore precluded from *in vivo* evaluation. Altogether, these experiments identified the FibraValve M as the design with the lowest regurgitation level in pulmonary hemodynamic conditions.

FibraValve in vivo performance and post-mortem evaluation

To assess *in vivo* function of the FibraValve M, transcatheter pulmonary valve replacements were performed in two sheep. Before implantation, the valves were crimped into a stent delivery system to enable a minimally invasive, transcatheter approach. The implantation procedure was successful in both animals, with immediate function of the FibraValves. Contrast angiography confirmed the correct valve positioning in the pulmonary location with the stent excluding the native leaflets and showing appropriate performance and hemodynamic loading of the valves (Figure 5A; Video S8). However, in one animal, acute migration of the FibraValve into the right ventricle was observed minutes after the implantation. This dislodgement was most likely caused by a size mismatch of the stented FibraValve and the native pulmonary artery.

The second animal remained hemodynamically stable during the entire implantation procedure and follow up without experiencing any peri-procedural complications. Fluoroscopy and 2D transesophageal echocardiography confirmed proper acute FibraValve performance, no stenosis, normal leaflet motion, and adequate opening-closing behavior (Figures 5B and S9; Video S9). There was a sufficient coaptation area and minimal central regurgitation (Figures S9 and S10; Video S10). The FibraValve was explanted after planned animal euthanasia, 1 h post-implant. Post-mortem macroscopic evaluation further confirmed appropriate positioning of the

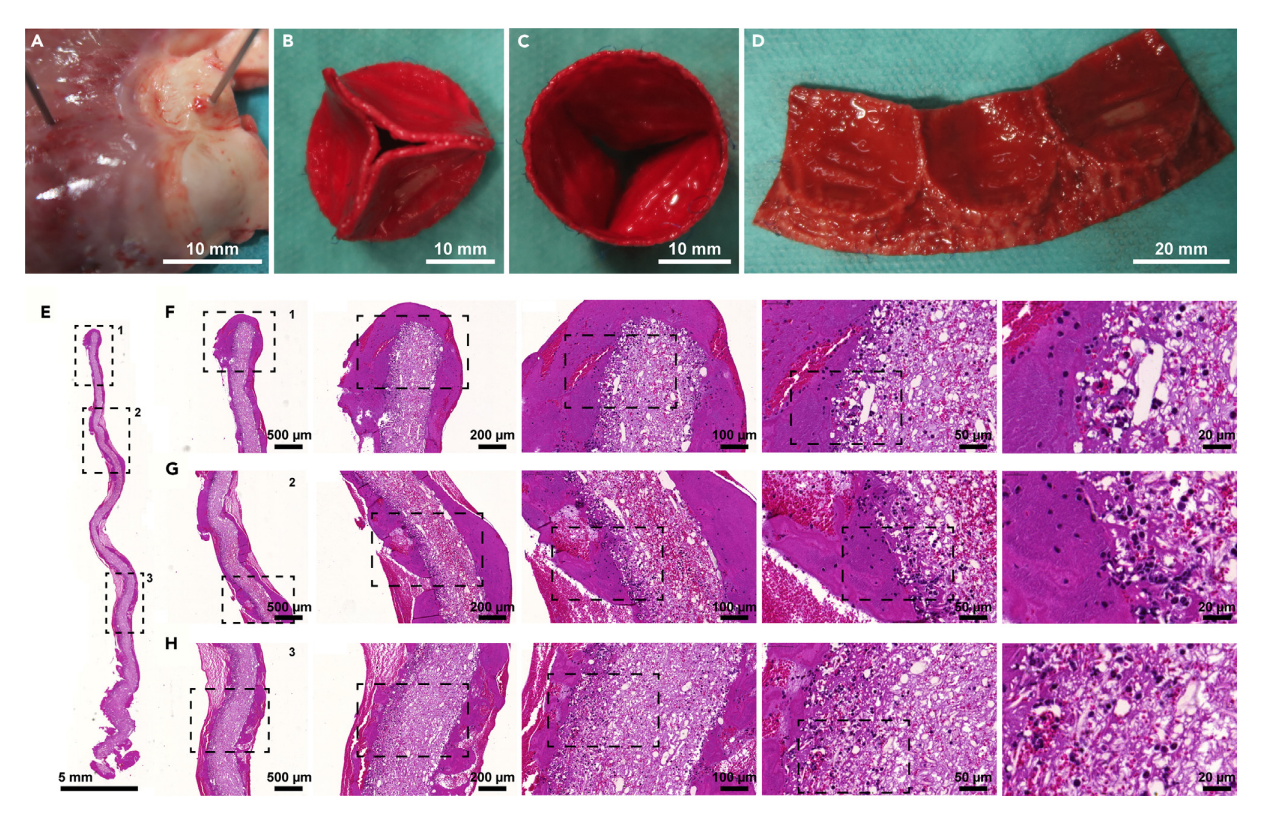


Figure 6. Post-mortem macroscopical and histological evaluation of implanted FibraValve

(A) Confirmation of correct positioning *in situ* as marked by the stent imprinting on the pulmonary artery and the presence of native leaflets. (B–D) Macroscopic appearance of explanted FibraValve upon harvesting (B, pulmonary side view; C, ventricular side view; D, cut open FibraValve pulmonary side view).

(E) Representative images of the H&E staining were performed on the valve cross-section. H&E staining shows retained leaflet morphology after 1 h in vivo

(F–H) Magnified images near the (F) tip, (G) midsection, and (H) base of the leaflet demonstrate the cellular infiltration throughout the entire leaflet thickness.

FibraValve in the pulmonary root without signs of stent migration, thrombus formation, leaflet tears, or rupture (Figures 6A–6D). Additionally, there were no macroscopic damages to the leaflet structure during the crimping and valve deployment procedures. Qualitative histological evaluations of the explanted FibraValve allowed the assessment of general valve morphology and cellular infiltration after 1 h. Fibrin deposition occurred on the surface of the valve (Figure 6E), while the leaflet structure was preserved. Early host cellular adhesion was observed across the leaflet's histological sections, with infiltration throughout the full thickness of the FibraValve leaflet (Figures 6F–6H). This cellular infiltration was predominantly characterized by the presence of erythrocytes and leukocytes. Overall, the FibraValve showed acute hemodynamic performance while allowing for initial cellular adhesion and infiltration without losing macroscopic leaflet shape and structure.

DISCUSSION

In this study, we tested FRJS as a manufacturing platform for fabricating heart valve scaffolds. This production method differs from electrospinning and 3D printing systems and allows for hierarchical control of valve scaffold features from the nanoscale





of the fibers to the centimeter scale of the valve's geometry. Here, FibraValves were spun in less than 10 min at production rates up to 0.2 g/min. Additionally, the microand nanofiber feature sizes in the FibraValves are consistent with native ECM. The use of 3D printing is limited as the micro- and nanoscale feature sizes require lengthy print times to produce full-size heart valves.³⁸ FRJS enables the fabrication of microand nanofibrous heart valve scaffolds in just minutes.

Compared with our group's previously reported JetValves, ³¹ FibraValves displayed deeper R in the leaflets. The deeper R is a result of the conformal deposition of FRJS and the embossing process performed after fiber spinning. Additionally, the FibraValve's longer LLs created larger coaptation areas than the JetValve, helping limit regurgitation during diastole. Both valves' materials, PLCL fibers (FibraValve) and poly-4-hydroxybutyrate (P4HB)/gelatin fibers (JetValve), possessed mechanical properties within the range of native valve leaflets. However, the PLCL fiber scaffolds showed an increased cellular infiltration rate and depth *in vitro*, key parameters when facilitating tissue remodeling. Another design difference is the presence of the JetValve's conduit surrounding the valve leaflets, a feature not included in the FibraValve. This conduit structure served as the connection point between the JetValve and the stent; however, it was removed from the FibraValve to enable potential future translation to the aortic valve position as well. In all, both valves intend to rapidly produce micro- and nanofibrous heart valve replacements, but the FibraValve displayed improvements in manufacturing, materials, and valve design.

The PLCL copolymer was synthesized to fabricate fiber scaffolds that more closely match the elastic modulus and strain recovery behavior of the native valve. Previously, PLCL scaffolds have shown advantages in terms of *in vivo* cellular infiltration and *de-novo*-synthesized ECM, further motivating their use in this study. ^{51,62–64} The synthesized PLCL fiber scaffolds demonstrated relatively soft mechanical properties compared with PCL controls and previously tested supramolecular approaches²⁷ but remained in the range of native valves (1–12 MPa). ⁵³ In efforts to provide initial insights about the impact of the scaffold properties on valve remodeling and regeneration, PLCL sheets were compared with PCL controls and tested *in vitro* for cellular adhesion after 2 days and for cellular infiltration after 1 and 4 weeks. For both cases, PLCL scaffolds performed better than PCL scaffolds, showing stronger adhesion and higher cellular infiltration. The combination of improved cellular adhesion and infiltration, as well as the material's strain recovery and elastic behavior, determined the selection of PLCL in the fabrication of FibraValves.

This study tested four different heart valve designs (S, M, L, and XL) fabricated with FRJS. All valves were subjected to pulmonary hemodynamic conditions in an *in vitro* pulse duplicator system. Corroborating a previous study, ³¹ the S design showed insufficient coaptation area, creating an opening at the center of the valve that was too large for the elastic properties of PLCL to compensate, leading to the highest regurgitation fraction. In contrast, the M design, although presenting a slight opening when positioned in the stent, exhibited complete closure and good coaptation under pulmonary pressures. Unfortunately, the FibraValves L and XL, designed to offset potential leaflet shrinkage previously observed with other TEHVs, ^{27,54} failed to function properly, as leaflets were prone to folding backward unpredictably. The poor leaflet motion of the L and XL designs led to high regurgitation levels *in vitro*. These observations suggest prosthetic designs' dependency on their building material properties, as decellularized matrix-based TEHVs of similar shapes and sizes displayed lower regurgitation levels under similar pressure conditions. ²² In this study, the FibraValve M design showed the lowest regurgitation levels



when using PLCL fibers as the building block, although changing the material of choice might yield different results when comparing different valve sizes' regurgitation levels.

To demonstrate valve functionality *in vivo*, we performed acute sheep studies using the FibraValve M design for transcatheter pulmonary valve replacement. Two stented FibraValves were successfully deployed in the pulmonary root, fully excluding the native valve. While both valves showed proper immediate function, one valve dislodged into the right ventricle. This displacement was most likely due to a size mismatch between the native annulus and the stented FibraValve and was not related to the structural integrity or performance of the valve. The second FibraValve performed as expected after delivery without peri- or post-procedural complications. Both leaflet motion and coaptation area were sufficient, with minimal central regurgitation, and there were no signs of paravalvular leakage or stenosis. During the 1 h implant, the PLCL scaffolds supported initial cellular attachment, with full-depth cellular infiltration into the scaffold as the polymer maintained its structure throughout the study duration. These *in vivo* findings were consistent with the *in vitro* study observations, suggesting the translatability of a rigorous *in vitro* experimentation process.

For the long-term success of these valves, the degradation kinetics of the synthetic scaffolds must complement the native tissue's infiltration and remodeling timescale in a way that maintains valve functionality. Previous work detailing chronic in vivo studies of PLCL implants yielded timescales to full degradation on the order of 12 months.⁵¹ However, the bioresorption rate can depend on the PCL:PLA ratio in the copolymer. Additionally, the monomer domains in the PLCL copolymer have been shown to degrade at different rates, as the faster degradation of the caprolactone moieties could potentially lead to changes in material behavior. Another variable affecting the degradation profile of FibraValves is the range of fiber diameters. Thicker fibers degrade more slowly, possibly offering continued structural support but also creating the potential for downstream reactions such as calcifications or leaflet contraction. Observations from these extended studies may inform polymer selection and design to maintain the desired valvular performance on a timescale that allows for complete native remodeling. To this end, chronic in vivo studies in the pulmonary valve position of large-animal models are necessary to gather the degradation kinetics in the unique, high-shear environment of the heart.

Conclusions

Current valve replacement options do not provide the necessary long-term solutions for pediatric patients with valvular diseases, while current manufacturing platforms are unable to produce effective regenerative replacements. Here, we show that FRJS can serve as a biofabrication method for implantable heart valves. The manufacturing platform recreates complex valve scaffolds and recapitulates the structure from nano- to centimeter scales in a customizable and cost- and time-efficient manner. Micro- and nanofiber-based FibraValves were fabricated from an elastic polymer, PLCL, into customized trileaflet valve geometries. These valves were spun in less than 10 min, showed adequate *in vitro* performance, and sustained acute *in vivo* functionality in a large-animal model. Moving forward, chronic studies will be used to assess the long-term efficacy of these synthetic scaffolds in promoting native-like tissue remodeling and maintaining one-way flow throughout the cardiac cycle. In summary, these results indicate that the FRJS could represent a viable





manufacturing platform for regenerative heart valve scaffolds and future medical implants.

EXPERIMENTAL PROCEDURES

Resource availability

Lead contact

Please contact Dr. Kevin Kit Parker (kkparker@g.harvard.edu) for any queries.

Materials availability

The materials generated in this study are available from the corresponding author upon request.

Data and code availability

The data and code are available upon reasonable request.

Materials

All reagents were commercially available and used without further modification unless otherwise stated. Materials for the synthesis of the PLCL polymer, including (3S)-cis-3,6-dimethyl-1,4-dioxane-2,5-dione; polycaprolactone diol ($M_n \sim 2,000$); tin(II) 2-ethylhexanoate; hexamethylene diisocyanate; 1,4-dioxane (anhydrous); diethyl ether (anhydrous); 1,1,1,3,3,3-hexafluoro-2-propanol (HFIP); and chloroform, were purchased from Sigma-Aldrich (St. Louis, MO, USA).

PLCL synthesis

A multiblock copolymer, PLCL (PLA:PCL, MW = \sim 220 kDa), was synthesized by polymerization of a PLA:PCL triblock copolymer via urethane bond formation using hexamethylene diisocyanate as linker. To form a PLA:PCL triblock copolymer, polycaprolactone diol (10 g) was dried under vacuum and mechanical stirring for 45 min at 90°C. After the polycaprolactone diol was dried, (3S)-cis-3,6-dimethyl-1,4-dioxane-2,5-dione (20 g) was added at 140°C, followed by the addition of tin(II) 2-ethylhexanoate (300 μ L) and stirring for 2 h. The obtained polymer was dissolved in chloroform (150 mL), precipitated from diethyl ether (1 L), and collected via filtration as a white solid. Under nitrogen atmosphere and mechanical stirring, the PLA:PCL triblock copolymer (20 g) was dissolved in anhydrous 1,4-dioxane (150 mL), followed by the addition of tin(II) 2-ethylhexanoate (300 μ L) and hexamethylene diisocyanate (400 μ L). The solution was heated up at 85°C and allowed to stir for 4 h. The polymer was precipitated from methanol (1 L) and filtered to yield a white solid. Lastly, the resulting white blocks were dried under vacuum prior to fiber production.

FRJS

The FRJS setup consists of a custom machined aluminum reservoir (diameter = 63 mm) perforated with three cylindrical orifices (diameter = 400 µm) (Figure S1). ³⁸ The reservoir's interior is hollow to allow air to travel through its opening (Figure S1). ³⁸ This custom-built reservoir was mounted to the shaft of a brushless motor oriented horizontally (E3000 Motor, Nakanishi, Tochigi, Japan), where the rotation speed ranged from 10,000 to 35,000 rpm. To create the focused air flow, pressurized air was directed into a 3D-printed piece that converged three air inputs into one focused stream that was directed through the rotating reservoir and toward the collection mandrel. (Figures 1C and S1). After synthesis of the polymer, PLCL was dissolved at 8% (w/v) in HFIP, loaded into 50 mL syringes, and extruded using an automated syringe pump (PHD Ultra, Harvard Apparatus, Holliston, MA, USA) at rates of 1–2 mL/min via tubing into the rotating reservoir.



PCL (\sim M_n 80,000, Sigma-Aldrich) was dissolved at 6% w/v in HFIP and spun under the same conditions. The FRJS system was placed in a ventilated gloved-box hood for solvent evaporation.

FibraValve manufacturing

FibraValve mandrels were designed with SolidWorks (Waltham, MA, USA) and 3D printed. Mandrels were then mounted to the shaft of a brushless motor, positioned 20 cm from the spinning reservoir, and rotated at 2,000 rpm to enable circumferential collection of PLCL fibers. FibraValves were fabricated with an average wall thickness of $\sim\!0.5$ mm. After spinning, FibraValves were placed in a ventilated chemical hood for at least 1 h to allow for solvent evaporation. The valves were then embossed using a 3D-printed mold complimentary to the FibraValve spinning target mold in order to deepen the R of the leaflet belly. Valves were embossed at 42°C for 2 h. Lastly, the valves were removed from the collection mandrel, and the leaflets were cut and separated with surgical scissors, revealing the final trileaflet shape (Figure S2).

Scanning electron microscopy (SEM)

Fiber scaffolds were removed from collectors, mounted on SEM stubs, and sputter coated with 10 nm platinum/palladium (Pt/Pd) using an EMS 300T Sputter Coater (Quorum Technologies, Lewes, UK) to minimize charge accumulation during imaging. The samples were imaged using a Zeiss SUPRA 55 field-emission SEM (Zeiss, Oberkochen, Germany) at a voltage of 5 kV.

Porosity measurements

Scaffold porosity was measured using a previously published liquid displacement method commonly used for porous tissue engineering scaffolds. ⁶⁵ Briefly, the scaffolds are submerged in a graduated cylinder with a liquid of a known volume (V_1), thereby increasing the volume to a new value that is the combination of V_1 and the volume of the fiber scaffold (V_2). Ethanol was used to penetrate the PCL and PLCL scaffolds without shrinking or swelling them. The ethanol-filled scaffolds were then removed from the cylinder, and the displaced liquid was measured (V_3). A porosity value could then be calculated using the following equation:

Porosity =
$$\frac{(V_1 - V_3)}{(V_2 - V_3)}$$
 (Equation 1)

Porosity values are reported as a percentage.

Mechanical testing

Mechanical properties were measured using a CellScale BioTester (Waterloo, ON, Canada) with 2.5 N load cells. Samples were cut in rectangular shapes (5 \times 20 mm) with a thickness of \sim 0.5 mm, hydrated with phosphate-buffered saline (PBS; Gibco, Thermo Fisher Scientific, Waltham, MA, USA), and mounted for uniaxial testing on the system using clamps. Tensile testing was performed up to 10% strain at a strain rate of 10% for 20 cycles. Measurements were performed at 37°C in PBS. Stress-strain curves were plotted for each sample, and Young's modulus was calculated in the linear region. The strain recovery was quantified as the strain percentage recovered prior to reaching the toe region, defined as the flat region of the stress-strain curve and low strains (Figure S5).

VIC harvesting

VICs were isolated from pulmonary heart valve leaflets of adult sheep obtained from a slaughterhouse (Blood Farms, Groton, MA, USA). Leaflet tissues were cut in small pieces and plated in Petri dishes with collagenase II (Sigma-Aldrich) at a





concentration of 425 U/mL for 5 min to remove the outer layer of valvular endothelial cells. The leaflets were then moved to fresh collagenase solutions and incubated for 3 h to remove the VICs. These VICs were plated and expanded until they reached confluency. Upon their confluency, the cells were passaged, expanded, and stored frozen until further use. Isolated cells were expanded in Advanced Dulbecco's modified Eagle medium/F-12 (Sigma-Aldrich), supplemented with 10% fetal bovine serum (Invitrogen, Waltham, MA, USA), 1% GlutaMAX (Invitrogen), and 1% penicillin-streptomycin (Invitrogen), and cultured in a cell incubator at 37°C and 5% CO₂.

In vitro cell infiltration studies

Fiber scaffolds were cut into rectangular shapes (5 × 20 mm) with a thickness of $\sim\!0.5$ mm, bonded to the bottom of 6-well plates using nail polish on both ends, and sterilized using UV for 30 min and 70% ethanol washes. To avoid bacterial and fungal contamination, the samples were then incubated with a solution of PBS, 10% penicillin-streptomycin, and 0.1% amphoteric solution for 30 min. Scaffolds were then rinsed and dried before being seeded with 1.5 M cells per square centimeter. To increase cell adhesion, cells were first seeded onto the scaffolds at high concentration in $\sim\!100~\mu\text{L}$ media. After 30 min of incubation, additional media were added to fully submerge the scaffolds. Thereafter, media were changed every 2 days for up to 4 weeks of culture.

Immunofluorescent staining

Scaffolds were washed twice in PBS (Gibco, Thermo Fisher Scientific), excised from their culture wells, and then fixed for 15 min in 4% paraformaldehyde (PFA; Electron Microscopy Sciences, Hatfield, PA, USA). Next, samples were washed 3 times in PBS and then incubated for 15 min in 0.05% Triton X-100 (Sigma-Aldrich). Samples were then washed 3 times with PBS. Next, scaffold samples were incubated in a solution of rabbit anti-vinculin (1:200 concentration in PBS; Abcam, Cambridge, UK) for 2 h at room temperature. Following primary incubation, samples were washed 3 times in PBS and incubated in a solution of rabbit immunoglobulin G (IgG; H + L) conjugated to Alexa Fluor 633 (at 1:200 concentration in PBS; Life Technologies, Carlsbad, CA, USA) for 2 h at room temperature. This solution also included Alexa Fluor 546 phalloidin (1:200 concentration; Life Technologies) and 4',6-diamidino-2-phenylindole dihydrochloride (DAPI; 1:200 concentration in PBS; Invitrogen). After secondary staining, samples were washed 3 times in PBS, mounted on glass coverslips in Prolong Gold anti-fade agent (Life Technologies), and imaged using a confocal microscope (Olympus Corporation, Tokyo, Japan).

Histology

Samples were fixed in 4% formalin and embedded in paraffin. Using a sliding microtome at room temperature, 10- to 20- μ m-thick slices were cut along the cross-section of scaffold samples. Finally, slices were stained with H&E prior to imaging.

In vitro FibraValve functionality tests

FibraValve samples were sutured onto 28 mm nitinol stents and positioned into custom-made holders for mounting in a pulse duplicator (ViVitro Labs, Victoria, BC, Canada). A cardiac waveform at 72 beats per minute and a pressure of 30 mmHg were set to recreate physiologic pulmonary conditions for testing the valve scaffolds. FibraValve functionality was tested for up to 7 days. Regurgitation and cardiac output could then be calculated to assess the overall performance of the prostheses.



Delivery system and crimping procedure

To enable transapical delivery of the FibraValves, a custom-made hydraulic delivery system was designed and manufactured by CARAG AG (Baar, Switzerland). The system comprised a 14 mm stainless-steel capsule to accommodate the loaded valve and a flexible delivery catheter. Delivery tests were performed on all FibraValves (n = 2) prior to implantation.

FibraValve in vivo transcatheter implantation and evaluation

The animal study was conducted at the Musculoskeletal Research Unit (MSRU) at the Vetsuisse Faculty of the University of Zurich. Animals received humane care in accordance with the "principles of laboratory animal care" and the "guide for the care and use of laboratory animals" of the National Institutes of Health. All procedures received the approval of the Cantonal Veterinary Office (license number ZH_111_2019) and were performed in accordance with the European Union guidelines (86/609/EEC) and Swiss Federal animal protection law and ordinance. Feasibility, safety, and acute performance of the FibraValves were evaluated in two sheep (white alpine sheep, 55–60 Kg) selected based on their annulus size (25.0 \pm 1 mm at peak systolic pressure).

Anesthesia was induced by intravenous injection of ketamine hydrochloride (Ketasol-100 ad us. vet.; Dr. E. Graeub AG, Bern, Switzerland; 3 mg/kg) in combination with midazolam (Dormicum; Roche Pharma AG, Reinach, Switzerland; 0.2 mg/kg) and propofol (Propofol-Lipuro 1%; B. Braun Medical AG, Sempach, Switzerland; 2–5 mg/kg). After intubation, anesthesia was maintained by positive pressure ventilation (fresh gas flow 1–1.5 L/min, 12–15 breaths/min, tidal volume 10–15 mL/kg, FiO2 0.5) of 2%–3% isoflurane in an oxygen-air mixture and a continuous infusion pump applying propofol (2–4 mg/kg/h). Throughout the procedure, the animals received a continuous intravenous infusion of sufentanil (Sufenta Forte, Janssen-Cilag AG, Zug, Switzerland; 0.05 mg/kg/h). Prior to valve delivery, animals were anticoagulated with a bolus injection of Na-Heparin (B. Braun Medical AG) to achieve an activated clotting time of 200–210 s.

The animals underwent surgery through anterolateral-thoracic access and antegrade approach at the third intercostal space. After mini-thoracotomy and pericardiotomy, the right ventricular apex was punctured with two purse-string sutures, and the valve delivery system was inserted under fluoroscopy (Allura FD 20/20, Philips Electronics, Amsterdam, the Netherlands). A baseline contrast angiography was performed to assess the native pulmonary valve and root. After correct positioning of the device, the valve was released under fluoroscopy guidance.

Planned follow ups for all animals (n = 2) were 60 min after implantation. Transesophageal echocardiography (iE33W xMATRIX Ultrasound, Philips Healthcare) and angiography were performed immediately after deployment and before euthanasia. A secondary device recorded a projection of the ultrasound equipment. The videos were processed using Adobe Premiere Pro (v.22.5.0, San Jose, CA, USA). Videos were stabilized using the Warp Stabilizer function to mitigate any drift and camera movement. The stabilization function's result setting was set to "no motion" to remove camera motion from the frames. Additionally, the method setting was "position," meaning that key features were held at constant positions from frame to frame during the stabilization process.





At the end of the follow-up period, the animals were euthanized with an overdose of Na-pentobarbital (75 mg/kg, intravenous delivery), and the heart was harvested for further analysis. The study did not include randomization or blind investigation.

Post-mortem evaluation

After euthanization, the heart was removed, and the FibraValve was macroscopically examined for tissue integrity and then processed using histological analysis (Benchmark, Ventana Medical Systems, Oro Valley, AZ, USA) to assess polymer composition and early cellular infiltration. Leaflet samples were fixed in 4% PFA and processed as previously described. The tissue sections were analyzed using H&E staining, imaged with bright-field microscopy, and assessed with Pannoramic Viewer software (3DHistech, Budapest, Hungary).

Statistical analyses

Statistical analyses were conducted using SigmaPlot (v.12.0, Systat Software, Chicago, IL, USA). One-way ANOVA on ranks with post hoc multiple comparison Dunn's test or Student's t test was used where appropriate for histological data analyses. Quantitative data are presented as mean \pm standard error of the mean, and significance was considered for p <0.05.

SUPPLEMENTAL INFORMATION

Supplemental information can be found online at https://doi.org/10.1016/j.matt. 2023.05.025.

ACKNOWLEDGMENTS

This work was sponsored by the John A. Paulson School of Engineering and Applied Sciences at Harvard University, the Wyss Institute for Biologically Inspired Engineering at Harvard University, and the Harvard Materials Research Science and Engineering Center (DMR-2011754). The work was also made possible by access to the facilities at the Center for Nanoscale Systems (CNS) at Harvard University, a member of the National Nanotechnology Infrastructure Network (1541959). S.E.M. was partly supported by the European Research Council (ERC) under the European Union's Horizon 2020 research and innovation program, grant agreement no. 852814 (TAVI4Life), and by the Swiss National Science Foundation, Spark grant no. CRSK-3_196717. P.Z. was supported by the ERC under the European Union's Horizon 2020 research and innovation program, grant agreement no. 852814 (TAVI4Life). E.S.F. was partly funded through the Swiss National Science Foundation (PZ00P3_180138). M.Y.E. was supported by the ERC under the European Union's Horizon 2020 research and innovation program, grant agreement no. 852814 (TAVI4Life). The authors would also like to thank Michael Rosnach for his help with schematics.

AUTHOR CONTRIBUTIONS

K.K.P., M.Y.E., and S.P.H. designed and supervised the study. S.E.M. and C.O.C. designed the FibraValves. M.M.P., H.C., and Q.L. fabricated the FibraValves. M.M.P. and L.C. designed and synthesized the polymer. S.E.M., M.M.P., C.O.C., and L.C. characterized the polymer. S.E.M. and E.M.C. performed *in vitro* studies. S.E.M., E.S.F., P.Z., N.C., and M.Y.E. performed the *in vivo* studies. S.E.M., C.O.C., and H.C. performed data analysis. S.E.M., M.M.P., C.O.C., H.C., and K.K.P. wrote the manuscript.



DECLARATION OF INTERESTS

S.P.H. is shareholder at Xeltis BV and LifeMatrix AG. M.Y.E. is a shareholder and advisor at LifeMatrix AG.

Received: January 30, 2023 Revised: April 19, 2023 Accepted: May 12, 2023 Published: June 7, 2023

REFERENCES

- Kumar, R.K., Antunes, M.J., Beaton, A., Mirabel, M., Nkomo, V.T., Okello, E., Regmi, P.R., Reményi, B., Sliwa-Hähnle, K., Zühlke, L.J., et al. (2020). Contemporary diagnosis and management of rheumatic heart disease: implications for closing the gap: a scientific statement from the American heart association. Circulation 142, E337–E357. https://doi.org/10.1161/CIR. 000000000000000921.
- Watkins, D.A., Johnson, C.O., Colquhoun, S.M., Karthikeyan, G., Beaton, A., Bukhman, G., Forouzanfar, M.H., Longenecker, C.T., Mayosi, B.M., Mensah, G.A., et al. (2017). Global, regional, and national burden of rheumatic heart disease, 1990-2015. N. Engl. J. Med. 377, 713–722. https://doi.org/10.1056/ NEJMOA1603693.
- 3. GBD 2017 Congenital Heart Disease Collaborators, Smith, A.G.C., Sable, C.A., Echko, M.M., Wilner, L.B., Olsen, H.E., Atalay, H.T., Awasthi, A., Bhutta, Z.A., Boucher, J.L.A., et al. (2020). Global, regional, and national burden of congenital heart disease, 1990–2017: a systematic analysis for the Global Burden of Disease Study 2017. Lancet. Child Adolesc. Health 4, 185–200. https://doi.org/10.1016/S2352-4642(19)30402-X.
- 4. Watkins, D.A., Beaton, A.Z., Carapetis, J.R., Karthikeyan, G., Mayosi, B.M., Wyber, R., Yacoub, M.H., and Zühlke, L.J. (2018). Rheumatic heart disease worldwide: JACC scientific expert panel. J. Am. Coll. Cardiol. 72, 1397–1416. https://doi.org/10.1016/J.JACC. 2018.06.063.
- Zilla, P., Brink, J., Human, P., and Bezuidenhout, D. (2008). Prosthetic heart valves: catering for the few. Biomaterials 29, 385–406. https://doi.org/10.1016/j. biomaterials.2007.09.033.
- Blum, K.M., Drews, J.D., and Breuer, C.K. (2018). Tissue-engineered heart valves: a call for mechanistic studies. Tissue Eng. Part B Rev. 24, 240–253. https://doi.org/10.1089/ten.teb. 2017.0425.
- Yacoub, M.H., and Takkenberg, J.J.M. (2005).
 Will heart valve tissue engineering change the world? Nat. Clin. Pract. Cardiovasc. Med. 2, 60–61. https://doi.org/10.1038/ncpcardio0112.
- Henaine, R., Roubertie, F., Vergnat, M., and Ninet, J. (2012). Valve replacement in children: a challenge for a whole life. Arch. Cardiovasc. Dis. 105, 517–528. https://doi.org/10.1016/j. acvd.2012.02.013.
- 9. Fioretta, E.S., von Boehmer, L., Motta, S.E., Lintas, V., Hoerstrup, S.P., and Emmert, M.Y.

- (2019). Cardiovascular tissue engineering: from basic science to clinical application. Exp. Gerontol. 117, 1–12. https://doi.org/10.1016/j.exqer.2018.03.022.
- Fioretta, E.S., Motta, S.E., Lintas, V., Loerakker, S., Parker, K.K., Baaijens, F.P.T., Falk, V., Hoerstrup, S.P., and Emmert, M.Y. (2021). Nextgeneration tissue-engineered heart valves with repair, remodelling and regeneration capacity. Nat. Rev. Cardiol. 18, 92–116. https://doi.org/ 10.1038/s41569-020-0422-8.
- Weber, B., Emmert, M.Y., and Hoerstrup, S.P. (2012). Stem cells for heart valve regeneration. Swiss Med. Wkly. 142, 1–11. https://doi.org/10. 4414/smw.2012.13622.
- Emmert, M.Y., Weber, B., Behr, L., Sammut, S., Frauenfelder, T., Wolint, P., Scherman, J., Bettex, D., Grünenfelder, J., Falk, V., and Hoerstrup, S.P. (2014). Transcatheter aortic valve implantation using anatomically oriented, marrow stromal cell-based, stented, tissueengineered heart valves: technical considerations and implications for translational cell-based heart valve concepts. Eur. J. Cardio. Thorac. Surg. 45, 61–68. https:// doi.org/10.1093/eicts/ezt243.
- Syedain, Z.H., Haynie, B., Johnson, S.L., Lahti, M., Berry, J., Carney, J.P., Li, J., Hill, R.C., Hansen, K.C., Thrivikraman, G., et al. (2021). Pediatric tri-tube valved conduits made from fibroblast-produced extracellular matrix evaluated over 52 weeks in growing lambs. Sci. Transl. Med. 13, eabb7225. https://doi.org/10. 1126/scitranslmed.abb7225.
- Motta, S.E., Lintas, V., Fioretta, E.S., Dijkman, P.E., Putti, M., Caliskan, E., Rodriguez Cetina Biefer, H., Lipiski, M., Sauer, M., Cesarovic, N., et al. (2019). Human cell-derived tissueengineered heart valve with integrated Valsalva sinuses: towards native-like transcatheter pulmonary valve replacements. npj Regen. Med. 4, 14. https://doi.org/10.1038/ s41536-019-0077-4.
- Syedain, Z., Reimer, J., Schmidt, J., Lahti, M., Berry, J., Bianco, R., and Tranquillo, R.T. (2015).
 6-Month aortic valve implantation of an off-the-shelf tissue-engineered valve in sheep.
 Biomaterials 73, 175–184. https://doi.org/10. 1016/j.biomaterials.2015.09.016.
- 16. Driessen-Mol, A., Emmert, M.Y., Dijkman, P.E., Frese, L., Sanders, B., Weber, B., Cesarovic, N., Sidler, M., Leenders, J., Jenni, R., et al. (2014). Transcatheter implantation of homologous "off-the-shelf" tissue-engineered heart valves with self-repair capacity: long-term functionality and rapid in vivo remodeling in

- sheep. J. Am. Coll. Cardiol. 63, 1320–1329. https://doi.org/10.1016/j.jacc.2013.09.082.
- Schmidt, D., Dijkman, P.E., Driessen-Mol, A., Stenger, R., Mariani, C., Puolakka, A., Rissanen, M., Deichmann, T., Odermatt, B., Weber, B., et al. (2010). Minimally-invasive implantation of living tissue engineered heart valves: a comprehensive approach from autologous vascular cells to stem cells. J. Am. Coll. Cardiol. 56, 510–520. https://doi.org/10.1016/j.jacc. 2010.04.024.
- Emmert, M.Y., Weber, B., Behr, L., Frauenfelder, T., Brokopp, C.E., Grünenfelder, J., Falk, V., and Hoerstrup, S.P. (2011).
 Transapical aortic implantation of autologous marrow stromal cell-based tissue-engineered heart valves: first experiences in the systemic circulation. JACC Cardiovasc. Interv. 4, 822–823. https://doi.org/10.1016/j.jcin.2011. 02.020.
- Weber, B., Dijkman, P.E., Scherman, J., Sanders, B., Emmert, M.Y., Grünenfelder, J., Verbeek, R., Bracher, M., Black, M., Franz, T., et al. (2013). Off-the-shelf human decellularized tissue-engineered heart valves in a non-human primate model. Biomaterials 34, 7269–7280. https://doi.org/10.1016/j.biomaterials.2013. 04.059.
- Lintas, V., Fioretta, E.S., Motta, S.E., Dijkman, P.E., Pensalfini, M., Mazza, E., Caliskan, E., Rodriguez, H., Lipiski, M., Sauer, M., et al. (2018). Development of a novel human cellderived tissue-engineered heart valve for transcatheter aortic valve replacement: an in vitro and in vivo feasibility study.
 J. Cardiovasc. Transl. Res. 11, 470–482. https:// doi.org/10.1007/s12265-018-9821-1.
- Motta, S.E., Fioretta, E.S., Dijkman, P.E., Lintas, V., Behr, L., Hoerstrup, S.P., and Emmert, M.Y. (2018). Development of an off-the-shelf tissueengineered sinus valve for transcatheter pulmonary valve replacement: a proof-ofconcept study. J. Cardiovasc. Transl. Res. 11, 182–191. https://doi.org/10.1007/s12265-018-9800-6.
- Emmert, M.Y., Schmitt, B.A., Loerakker, S., Sanders, B., Spriestersbach, H., Fioretta, E.S., Bruder, L., Brakmann, K., Motta, S.E., Lintas, V., et al. (2018). Computational modeling guides tissue-engineered heart valve design for longterm in vivo performance in a translational sheep model. Sci. Transl. Med. 10, eaan4587. https://doi.org/10.1126/scitranslmed.aan4587.
- 23. Emmert, M.Y., Weber, B., Wolint, P., Behr, L., Sammut, S., Frauenfelder, T., Frese, L., Scherman, J., Brokopp, C.E., Templin, C., et al. (2012). Stem cell-based transcatheter aortic





- valve implantation: first experiences in a preclinical model. JACC Cardiovasc. Interv. 5, 874–883. https://doi.org/10.1016/j.jcin.2012. 04.010.
- Capulli, A.K., MacQueen, L.A., Sheehy, S.P., and Parker, K.K. (2016). Fibrous scaffolds for building hearts and heart parts. Adv. Drug Deliv. Rev. 96, 83–102. https://doi.org/10.1016/ j.addr.2015.11.020.
- Jana, S., Tranquillo, R.T., and Lerman, A. (2016). Cells for tissue engineering of cardiac valves.
 J. Tissue Eng. Regen. Med. 10, 804–824. https://doi.org/10.1002/TERM.2010.
- Huygens, S.A., A Goossens, L.M., van Erkelens, J.A., M Takkenberg, J.J., and Rutten-van Mölken, M.P. (2018). How much does a heart valve implantation cost and what are the health care costs afterwards? Valvular heart disease. Open Hear 5, 672. https://doi.org/10.1136/ openhrt-2017-000672.
- Kluin, J., Talacua, H., Smits, A.I.P., Emmert, M.Y., Brugmans, M.C.P., Fioretta, E.S., Dijkman, P.E., Söntjens, S.H.M., Duijvelshoff, R., Dekker, S., et al. (2017). In situ heart valve tissue engineering using a bioresorbable elastomeric implant - from material design to 12 months follow-up in sheep. Biomaterials 125, 101–117. https://doi.org/10.1016/j. biomaterials.2017.02.007.
- De Kort, B.J., Marzi, J., Brauchle, E.M., Lichauco, A.M., Bauer, H.S., Serrero, A., Dekker, S., Cox, M.A.J., Schoen, F.J., Schenke-Layland, K., et al. (2021). Inflammatory and regenerative processes in bioresorbable synthetic pulmonary valves up to two years in sheep – spatiotemporal insights augmented by Raman microspectroscopy. Acta Biomater. 135, 243–259. https://doi.org/10.1016/j.actbio. 2021.09.005.
- Bennink, G., Torii, S., Brugmans, M., Cox, M., Svanidze, O., Ladich, E., Carrel, T., and Virmani, R. (2018). A novel restorative pulmonary valved conduit in a chronic sheep model: mid-term hemodynamic function and histologic assessment. J. Thorac. Cardiovasc. Surg. 155, 2591–2601.e3. https://doi.org/10.1016/j.jtcvs. 2017.12.046.
- Uiterwijk, M., Smits, A.I.P., van Geemen, D., van Klarenbosch, B., Dekker, S., Cramer, M.J., van Rijswijk, J.W., Lurier, E.B., Di Luca, A., Brugmans, M.C.P., et al. (2020). In situ remodeling overrules bioinspired scaffold architecture of supramolecular elastomeric tissue-engineered heart valves. JACC. Basic Transl. Sci. 5, 1187–1206. https://doi.org/10. 1016/J.JACBTS.2020.09.011.
- Capulli, A.K., Emmert, M.Y., Pasqualini, F.S., Kehl, D., Caliskan, E., Lind, J.U., Sheehy, S.P., Park, S.J., Ahn, S., Weber, B., et al. (2017).
 JetValve: rapid manufacturing of biohybrid scaffolds for biomimetic heart valve replacement. Biomaterials 133, 229–241. https://doi.org/10.1016/j.biomaterials.2017. 04 033
- Zhang, X., Xu, B., Puperi, D.S., Wu, Y., West, J.L., and Grande-Allen, K.J. (2015). Application of hydrogels in heart valve tissue engineering. J. Long Term Eff. Med. Implants 25, 105–134. https://doi.org/10.1615/ jlongtermeffmedimplants.2015011817.

- Jana, S., and Lerman, A. (2015). Bioprinting a cardiac valve. Biotechnol. Adv. 33, 1503–1521. https://doi.org/10.1016/j.biotechadv.2015. 07.006.
- Szentivanyi, A., Chakradeo, T., Zernetsch, H., and Glasmacher, B. (2011). Electrospun cellular microenvironments: understanding controlled release and scaffold structure. Adv. Drug Deliv. Rev. 63, 209–220. https://doi.org/10.1016/j. addr.2010.12.002.
- Stasiak, J.R., Serrani, M., Biral, E., Taylor, J.V., Zaman, A.G., Jones, S., Ness, T., De Gaetano, F., Costantino, M.L., Bruno, V.D., et al. (2020). Design, development, testing at ISO standards and in vivo feasibility study of a novel polymeric heart valve prosthesis. Biomater. Sci. 8, 4467– 4480. https://doi.org/10.1039/D0BM00412J.
- Stasiak, J., Brubert, J., Serrani, M., Nair, S., De Gaetano, F., Costantino, M.L., and Moggridge, G.D. (2014). A bio-inspired microstructure induced by slow injection moulding of cylindrical block copolymers. Soft Matter 10, 6077–6086. https://doi.org/10.1039/ C4SM00884G.
- Maxson, E.L., Young, M.D., Noble, C., Go, J.L., Heidari, B., Khorramirouz, R., Morse, D.W., and Lerman, A. (2019). In vivo remodeling of a 3D-Bioprinted tissue engineered heart valve scaffold. Bioprinting 16, e00059. https://doi. org/10.1016/j.bprint.2019.e00059.
- Chang, H., Liu, Q., Zimmerman, J.F., Lee, K.Y., Jin, Q., Peters, M.M., Rosnach, M., Choi, S., Kim, S.L., Ardoña, H.A.M., et al. (2022). Recreating the heart's helical structurefunction relationship with focused rotary jet spinning. Science 377, 180–185. https://doi. org/10.1126/SCIENCE.ABL6395.
- Sohier, J.Ô., Carubelli, I., Sarathchandra, P., Latif, N., Chester, A.H., and Yacoub, M.H. (2014). The potential of anisotropic matrices as substrate for heart valve engineering. Biomaterials 35, 1833–1844. https://doi.org/10. 1016/J.BIOMATERIALS.2013.10.061.
- Chester, A.H., El-Hamamsy, I., Butcher, J.T., Latif, N., Bertazzo, S., and Yacoub, M.H. (2014). The living aortic valve: from molecules to function. Glob Cardiol Sci Pr 2014, 52–77. https://doi.org/10.5339/gcsp.2014.11.
- Balachandran, K., Sucosky, P., and Yoganathan, A.P. (2011). Hemodynamics and mechanobiology of aortic valve inflammation and calcification. Int. J. Inflam. 2011, 263870. https://doi.org/10.4061/2011/263870.
- Chang, H., Xu, J., Macqueen, L.A., Aytac, Z., Peters, M.M., Zimmerman, J.F., Xu, T., Demokritou, P., and Parker, K.K. (2022). Highthroughput coating with biodegradable antimicrobial pullulan fibres extends shelf life and reduces weight loss in an avocado model. Nat. Food 3, 428–436. https://doi.org/10.1038/ s43016-022-00523-w.
- Gonzalez, G.M., MacQueen, L.A., Lind, J.U., Fitzgibbons, S.A., Chantre, C.O., Huggler, I., Golecki, H.M., Goss, J.A., and Parker, K.K. (2017). Production of synthetic, para-aramid and biopolymer nanofibers by immersion rotary jet-spinning. Macromol. Mater. Eng. 302, 1600365. https://doi.org/10.1002/mame. 201600365.

- Deravi, L.F., Sinatra, N.R., Chantre, C.O., Nesmith, A.P., Yuan, H., Deravi, S.K., Goss, J.A., MacQueen, L.A., Badrossamy, M.R., Gonzalez, G.M., et al. (2017). Design and fabrication of fibrous nanomaterials using pull spinning. Macromol. Mater. Eng. 302, 1600404. https:// doi.org/10.1002/mame.201600404.
- Badrossamay, M.R., McIlwee, H.A., Goss, J.A., and Parker, K.K. (2010). Nanofiber assembly by rotary jet-spinning. Nano Lett. 10, 2257–2261. https://doi.org/10.1021/nl101355x.
- Liu, W., Zhang, L.P., Xu, M., Zeng, H.Z., Zeng, Q.S., Chen, H.L., Liu, Q., Tang, S.J., and Hu, B. (2018). A viscoelastic beam theory of polymer jets with application to rotary jet spinning. Extrem. Mech. Lett. 19, 37–41. https://doi.org/ 10.1016/j.eml.2018.10.005.
- Mellado, P., McIlwee, H.A., Badrossamay, M.R., Goss, J.A., Mahadevan, L., and Kit Parker, K. (2011). A simple model for nanofiber formation by rotary jet-spinning. Appl. Phys. Lett. 99, 203107. https://doi.org/10.1063/1.3662015.
- Golecki, H.M., Yuan, H., Glavin, C., Potter, B., Badrossamay, M.R., Goss, J.A., Phillips, M.D., and Parker, K.K. (2014). Effect of solvent evaporation on fiber morphology in rotary jet spinning. Langmuir 30, 13369–13374. https:// doi.org/10.1021/la5023104.
- Leopold, J.A. (2012). Cellular mechanisms of aortic valve calcification. Circ. Cardiovasc. Interv. 5, 605–614. https://doi.org/10.1161/ CIRCINTERVENTIONS.112.971028.
- Omer, S., Forgách, L., Zelkó, R., and Sebe, I. (2021). Scale-up of electrospinning: market overview of products and devices for pharmaceutical and biomedical purposes. Pharmaceutics 13, 1–21. https://doi.org/10. 3390/PHARMACEUTICS13020286.
- 51. Zhu, M., Wu, Y., Li, W., Dong, X., Chang, H., Wang, K., Wu, P., Zhang, J., Fan, G., Wang, L., et al. (2018). Biodegradable and elastomeric vascular grafts enable vascular remodeling. Biomaterials 183, 306–318. https://doi.org/10.1016/j.biomaterials.2018.08.063.
- Christie, G.W. (1992). Anatomy of aortic heart valve leaflets: the influence of glutaraldehyde fixation on function. Eur. J. Cardio. Thorac. Surg. 6, S25–S32; discussion S33. https://doi. org/10.1093/ejcts/6.Supplement_1.S25.
- Hasan, A., Ragaert, K., Swieszkowski, W., Selimović, S., Paul, A., Camci-Unal, G., Mofrad, M.R.K., and Khademhosseini, A. (2014). Biomechanical properties of native and tissue engineered heart valve constructs. J. Biomech. 47, 1949–1963. https://doi.org/10.1016/j. jbiomech.2013.09.023.
- 54. Serruys, P.W., Miyazaki, Y., Katsikis, A., Abdelghani, M., Leon, M.B., Virmani, R., Carrel, T., Cox, M., Onuma, Y., and Soliman, O.I.I. (2017). Restorative valve therapy by endogenous tissue restoration: tomorrow's world? Reflection on the EuroPCR 2017 session on endogenous tissue restoration. EuroIntervention. 13. Aa68-aa77. https://doi. org/10.4244/eij-d-17-00509.
- 55. Fioretta, E.S., Lintas, V., Mallone, A., Motta, S.E., von Boehmer, L., Dijkman, P.E., Cesarovic, N., Caliskan, E., Rodriguez Cetina Biefer, H., Lipiski, M., et al. (2020). Differential leaflet remodeling of bone marrow cell pre-seeded



- versus nonseeded bioresorbable transcatheter pulmonary valve replacements. JACC. Basic Transl. Sci. 5, 15–31. https://doi.org/10.1016/j. jacbts.2019.09.008.
- Jana, S., Bhagia, A., and Lerman, A. (2019). Optimization of polycaprolactone fibrous scaffold for heart valve tissue engineering. Biomed. Mater. 14, 065014. https://doi.org/10. 1088/1748-605X/AB3D24.
- Lutter, G., Puehler, T., Cyganek, L., Seiler, J., Rogler, A., Herberth, T., Knueppel, P., Gorb, S.N., Sathananthan, J., Sellers, S., et al. (2022). Biodegradable poly-e-caprolactone scaffolds with ECFCs and iMSCs for tissue-engineered heart valves. Int. J. Mol. Sci. 23, 527. https://doi. org/10.3390/IJMS23010527.
- Cohn, D., and Salomon, A.H. (2005). Designing biodegradable multiblock PCL/PLA thermoplastic elastomers. Biomaterials 26, 2297–2305. https://doi.org/10.1016/j. biomaterials.2004.07.052.
- 59. Chantre, C.O., Hoerstrup, S.P., and Parker, K.K. (2019). Engineering biomimetic and

- instructive materials for wound healing and regeneration. Curr. Opin. Biomed. Eng. 10, 97–106. https://doi.org/10.1016/j.cobme. 2019.04.004.
- Sanders, B., Loerakker, S., Fioretta, E.S., Bax, D.J.P., Driessen-Mol, A., Hoerstrup, S.P., and Baaijens, F.P.T. (2016). Improved geometry of decellularized tissue engineered heart valves to prevent leaflet retraction. Ann. Biomed. Eng. 44, 1061–1071. https://doi.org/10.1007/ s10439-015-1386-4
- 61. Motta, S.E., Fioretta, E.S., Lintas, V., Dijkman, P.E., Hilbe, M., Frese, L., Cesarovic, N., Loerakker, S., Baaijens, F.P.T., Falk, V., et al. (2020). Geometry influences inflammatory host cell response and remodeling in tissue-engineered heart valves in-vivo. Sci. Rep. 10, 19882. https://doi.org/10.1038/s41598-020-76322-9.
- 62. Jeong, S.I., Kim, B.-S., Lee, Y.M., Ihn, K.J., Kim, S.H., and Kim, Y.H. (2004). Morphology of elastic poly(I-lactide-co-ε-caprolactone) copolymers and in vitro and in vivo

- degradation behavior of their scaffolds. Biomacromolecules 5, 1303–1309. https://doi.org/10.1021/bm049921i.
- 63. Jeong, S.I., Kim, S.H., Kim, Y.H., Jung, Y., Kwon, J.H., Kim, B.-S., and Lee, Y.M. (2004). Manufacture of elastic biodegradable PLCL scaffolds for mechano-active vascular tissue engineering. J. Biomater. Sci. Polym. Ed. 15, 645–660. https://doi.org/10.1163/156856204323046906.
- 64. Jeong, S.I., Kim, B.-S., Kang, S.W., Kwon, J.H., Lee, Y.M., Kim, S.H., and Kim, Y.H. (2004). In vivo biocompatibilty and degradation behavior of elastic poly(L-lactide-co-epsilon-caprolactone) scaffolds. Biomaterials 25, 5939–5946. https://doi.org/10.1016/j.biomaterials. 2004.01.057.
- Zhang, Y., and Zhang, M. (2001). Synthesis and characterization of macroporous chitosan/ calcium phosphate composite scaffolds for tissue engineering. J. Biomed. Mater. Res. 55, 304–312. https://doi.org/10.1002/ 1097-4636.